Journal of Alloys and Compounds 659 (2016) 15–22

Contents lists available at ScienceDirect

Journal of Alloys and Compounds

journal homepage: http://www.elsevier.com/locate/jalcom

Nitrogen and yttrium co-doped mesoporous titania photoanodes applied in DSSCs

Weiqi Wang, Yangqiao Liu*, Jing Sun**, Lian Gao

The State Key Laboratory of High Performance and Superfine Microstructure, Shanghai Institute of Ceramics, Chinese Academy of Sciences, 1295 Dingxi Road, Shanghai 200050, PR China

ARTICLE INFO

Article history:
Received 22 September 2015
Received in revised form
18 October 2015
Accepted 26 October 2015
Available online 30 October 2015

Keywords:
Dye-sensitized solar cells
Sol–gel method
Y,N co-doped TiO_2

ABSTRACT

In this paper, we synthesized Y, N co-doped TiO_2 nanoparticles via a simple sol–gel method. The incorporated yttrium and nitrogen increased the BET surface area and porosity of the nanoparticles, as the sample 100-300-0.5 reached 105.9 m^2/g, which largely improved the dye adsorption ability and obviously enhanced the J_{sc}. By optimizing doping amount of TiO_2, sample 100-300-0.5, for which the doping concentration characterized by XPS survey was 0.30% and 0.48% of yttrium and nitrogen, respectively, showed the best efficiency of 5.41% without any post-treatments on the electrode, 18% higher than the un-doped sample100-0-0. According to EIS measurements, charge transfer resistance could decrease to as low as 39.3Ω in the co-doped samples, which was almost half of the un-doped TiO_2. This work may open up more studies to apply co-doped TiO_2 in photovoltaic cells.

1. Introduction

In recent years, dye-sensitized solar cells (DSSCs), featuring new dyes, semiconducting materials and electrolytes, have shown great potential in high efficiency solar energy conversion [1–4]. Different semiconductors with various morphologies and crystal structures [5–11] have been fabricated into photoanodes to improve the cell performance.

As a crucial part of DSSCs, researchers have tried many different techniques [12–14] to enhance the charge transport for improving performance, among which doping TiO_2 with metal element cations is a common method. For example, M. J. Robles-Aguila et al. [15] incorporated Ni^{2+} into TiO_2 by an ultrasonic-assisted sol–gel method; F. Q. Huang et al. [16] synthesized Nb^{5+} doped TiO_2 powders through a hydrothermal process, improving the cell performance of ca. 18% compared to the un-doped cell; M. Liu et al. [17] synthesized Ca^{2+} doped TiO_2 nanorod arrays to form the photoanodes of DSSCs. Other metals as Al, Fe, Ga, La, and *etc.* [18–21] are also applied to dope the TiO_2, tailoring the band gap and electrical conductivity of the material.

Additionally, not only limited in metal element cation doping, but studies with nonmetal anion doping are widely reported as well. Elements as N, C, F, S [22–25] have been introduced to modifying the optical properties of TiO_2. Ma et al.'s work [26–28] with N-doped TiO_2 based DSSCs have extensively shown great long term stability and better conversion efficiencies. By substituting N doped TiO_2 for un-doped electrodes, they achieved higher incident photo-current efficiency (IPCE) and retarded electron recombination.

However, single doped TiO_2 may face several issues. For example, doping with transitional metals may reduce the thermal stability of nanoparticles [29], while doping with non-metal anions may create trap states near valence band that increase the recombination in the cell [30]. Consequently, some researchers synthesized co-doped TiO_2 based photocatalysts [31,32] and electrodes of lithium-ion batteries [33], trying to modify TiO_2 by utilizing both the cation and anion doping. However, up to now, no study has been taken on using codoped TiO_2 as DSSC photoanodes. Herein, we chose yttrium as the doping cation for its success in enhancing the charge collection efficiency of DSSCs and perovskite solar cells [34,35], and together with popularly studied nitrogen as the doping anion to synthesize yttrium and nitrogen co-doped TiO_2 nanoparticles through a simple sol–gel method using familiar precursors as urea and yttrium chloride. Then we prepared DSSCs based on doped TiO_2 thin films, to determine the doping effect the

* Corresponding author.
** Corresponding author.
E-mail addresses: yqliu@mail.sic.ac.cn (Y. Liu), jingsun@mail.sic.ac.cn (J. Sun).

http://dx.doi.org/10.1016/j.jallcom.2015.10.254
0925-8388/

structural, electronic properties of pristine TiO_2 and the photovoltaic performances of DSSCs.

2. Material and methods

2.1. Material synthesis

Titanium(IV) butoxide (TBOT, 98%), urea, acetic acid, nitric acid (65%) and anhydrous ethanol were obtained from Sinopharm. Yttrium chloride (YCl_3, 99.9%) was purchased from Alfa. All reagents and solvents were used as received. Nanocrystalline TiO_2 co-doped with nitrogen and yttrium was synthesized through a modified simple sol–gel method [35]. A certain amount of YCl_3 and urea were dissolved into 160 ml deionized water (DI water) to form mixture solution A. Then the mixture solution B of 6.5 g acetic acid and 31 g TBOT was dropwise added into the mixture solution A under vigorous stirring. After stirred for another hour till TBOT fully hydrolyzed, 1 ml nitric acid was added into the suspension and it was heated to 80 °C for 75 min to form a translucent TiO_2 sol. Then the sol was poured into Teflon autoclave and subjected to gelation at 180 °C for 6 h. Finally the precipitate was rinsed with DI water and ethanol, dried in a vacuum oven overnight. The samples were marked as Ti(a)–N(b)–Y(c), where a, b and c stood for nominal molar ratio of Ti, N and Y added in the precursor solutions. However, as XPS survey indicated, there was a discrepancy between the dopants added in the precursors and TiO_2 nanoparticles synthesized. The obtained TiO_2 nanoparticles were mixed with terpineol, ethyl cellulose ethanol solution to prepare a TiO_2 paste according to a previous literature [36].

2.2. Assembly of DSSCs

The photoanode was assembled by coating the paste onto the FTO substrate by doctor-blade and further calcined at 450 °C for half an hour. Then the photoanode was immersed for 24 h in a ruthenium dye solution (*cis*-bis(isothiocyanato)bis(2,2′-bipyridyl-4,4′-dicarboxylato)-ruthenium(II) bis-tetrabutylammonium (N-719 dye) that was dissolved in acetonitrile/tert-butanol with a concentration of 0.3 mM). The anode was then taken out, rinsed with acetonitrile and dried. After that, one drop of electrolyte, composed of 0.1 M lithium iodide (LiI), 0.6 M tetrabutylammonium iodide (TBAI), 0.05 M iodine (I_2), and 0.5 M 4-tert-butylpyridine (tBP) dissolved in acetonitrile, was deposited onto the electrode. A sputtered platinum FTO counter electrode was clipped on to form a photovoltaic cell for further characterization.

2.3. Characterizations

Compositions of the samples were investigated by X-ray diffraction (XRD, D/max 2550V, Rigaku Tokyo) and Raman spectroscopy (DXR Raman Microscope with an excitation length of 532 nm, Thermo Fisher). The morphology was characterized with field emission electron transmission microscope (FETEM, JEM-2100F). The UV–vis spectra and dye adsorption amount were recorded by Lamda 950, Perkin Elmer. Photoluminescence emission spectra were performed by FluoroMax-4 fluorescence spectrometer, using the excitation wavelength of 325 nm. XPS measurements were performed on ESCAlab 250, Thermo Fisher. The photocurrent–voltage (I–V) curves were recorded by Keithley 2400 m under illumination of 100 mW/cm^2 AM 1.5G simulated sunlight, which was performed by an Oriel-Newport Xe lamp. Electrochemical impedance spectroscopy (EIS) measurements were carried out on a CHI 660D electrochemical workstation and further fitted by Z-view.

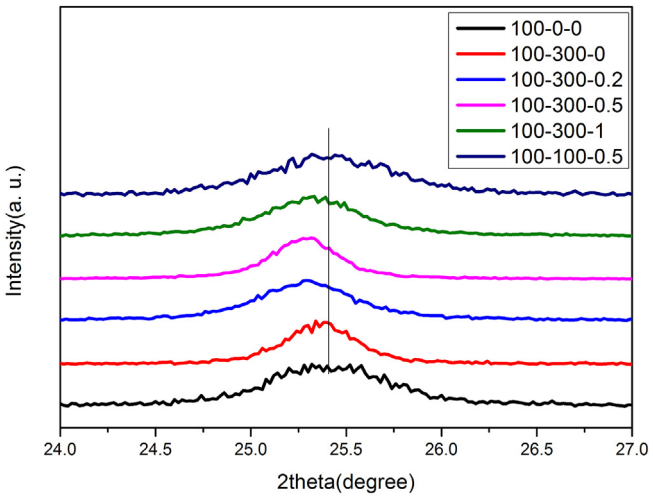

Fig. 1. Detailed XRD patterns of TiO_2 (101).

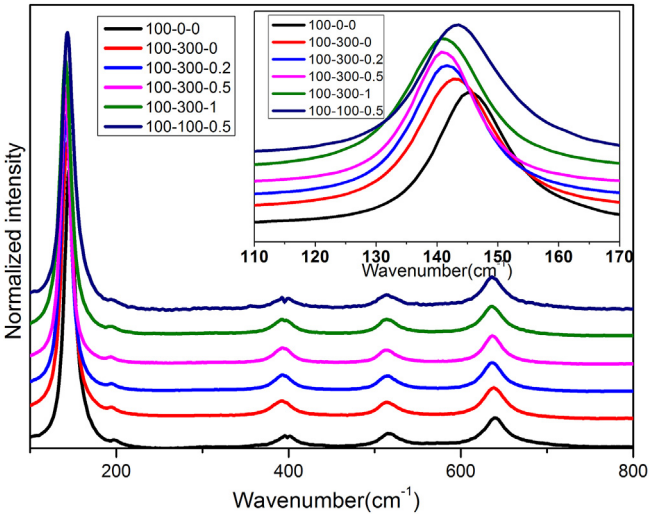

Fig. 2. Raman spectra of synthesized TiO_2 nanoparticles. Detailed E_g modes near 142 cm^{-1} are shown in the inset.

3. Results and discussion

3.1. Morphologies and crystal structures of Y, N co-doped TiO_2 powders

The XRD patterns of the synthesized TiO_2 nanoparticles are shown in Fig. S1. As shown in the XRD patterns, the synthesized TiO_2 nanoparticles are crystalline materials. The peak positions and their respective orientations are consistent with the JCPDS card No.21-1272, which indicates that the TiO_2 nanoparticles own an anatase structure. Besides, no yttrium oxide peaks in the patterns could be found, which indicates the negligible amount of impurities in all of the samples. Furthermore, the detailed XRD patterns of synthesized TiO_2 powders around 25° are shown in Fig. 1. As Fig. 1 illustrates, the (101) diffraction angle of 100-0-0 is 25.42°, while it is 25.34° for the nitrogen single doped 100-300-0. In particular, in yttrium and nitrogen co-doped samples, the diffraction angles are 25.31°, 25.31°, 25.33° and 25.32° for 100-300-0.2, 100-300-0.5, 100-300-1 and 100-100-0.5, respectively. According to the Bragg equation $n\lambda = 2d\sin\theta$, the diffraction angle decrease might indicate the lattice distortion due to larger ions doping into the crystal

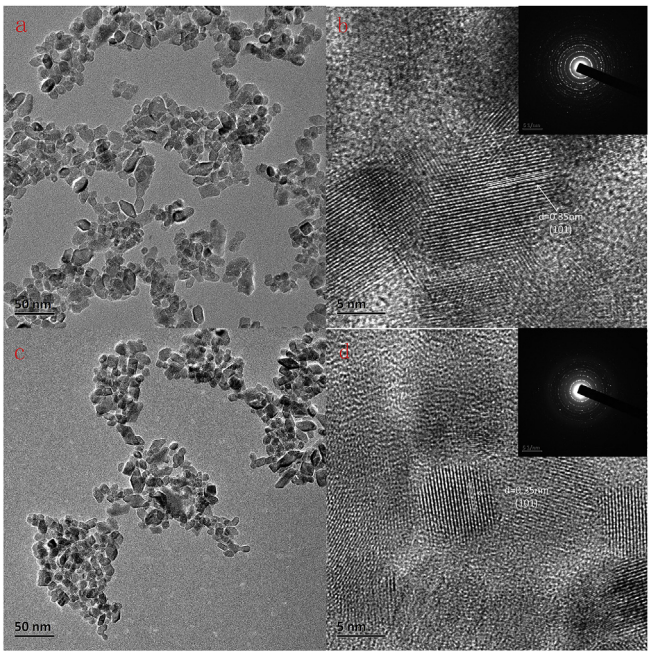

Fig. 3. TEM &HRTEM images of 100-0-0 (a and b), 100-300-0.5 (c and d), respectively. Inset images are the SAED patterns of the corresponding samples.

(calculated d(101) is 3.501 Å for 100-0-0 and 3.516 Å for doped samples). Moreover, Raman spectroscopy is another potent method to investigate the microstructure of oxides. In Fig. 2, Raman spectra of these six samples are shown. Each spectrum contains one strongest band near 141 cm^{-1} and four weaker bands at 194.0, 393.0, 513.3 and 636.6 cm^{-1}, which can be assigned to five Raman-active modes of anatase phase with symmetries of E_g, E_g, B_{1g}, A_{1g} and E_g, respectively [37]. Similarly, no yttrium oxide peaks are found in Raman spectra, which is accordant with the XRD patterns. As shown in the inset of Fig. 2, the strongest E_g mode of 100-0-0 is at 144 cm^{-1}, while the E_g peak of N doped one is 142 cm^{-1}. Furthermore, when the yttrium doping amount increases, i.e., as the samples 100-300-0.2 to 100-300-1 show, the E_g mode red-shifts become more obvious. The E_g peak location difference between 100-0-0 and 100-300-1 almost reached 4 cm^{-1} in this experiment. Since the peak location red-shifts can be attributed to the phonon frequency decrease caused by lattice expansion [38], we may also infer that yttrium and nitrogen are successfully incorporated into the crystal.

The morphologies of pure (100-0-0) and Y, N co-doped (100-300-0.5) samples characterized by TEM and HRTEM are shown in Fig. 3. Compared to images of pure TiO_2 (as shown in Fig. 3a and b), the size and morphology of Y, N co-doped TiO_2 (as shown in Fig. 3c and d) are retained after being doped with urea and yttrium chloride. From Fig. 3a and c, both samples comprises agglomerated nanoparticles, and the grain size of synthesized TiO_2 nanoparticles are estimated to be both ca. 15 nm. And from Fig. 3b and d HRTEM images, the observed spacing from neighboring crystal fringes is obtained as ca. 3.5 Å for the (101) plane of anatase crystal, which corresponds with XRD results.

The change of precursors doping level also affects the surface properties of the nanoparticles. Measurements of nitrogen isothermal adsorption/desorption experiments gave information of the Brunauer–Emmett–Teller (BET) surface area of the nanoparticles. Table S1 summarized the BET specific surface area and pore data of all six samples (Fig. S2 shows the isothermal curve and pore distribution of 100-300-0.5). The isothermal curve illustrates a typical type IV isotherm, representing mesoporous structures of synthesized nanoparticles. According to Table S1, after nitridation of pure TiO_2, the calculated surface area increases from 66.6 m^2/g of 100-0-0 to 97.5 m^2/g of 100-300-0. Moreover, as the yttrium precursors are added to co-dope with nitrogen, the highest surface area reached 121.7 m^2/g of 100-300-1, almost twice of the pure one. As the particle sizes and average pore diameters remained the same, the enhanced surface area should result from the higher porosity of the doped samples. A much bigger surface area may enhance the dye adsorption ability of the nanoparticles, favoring a higher DSSC performance.

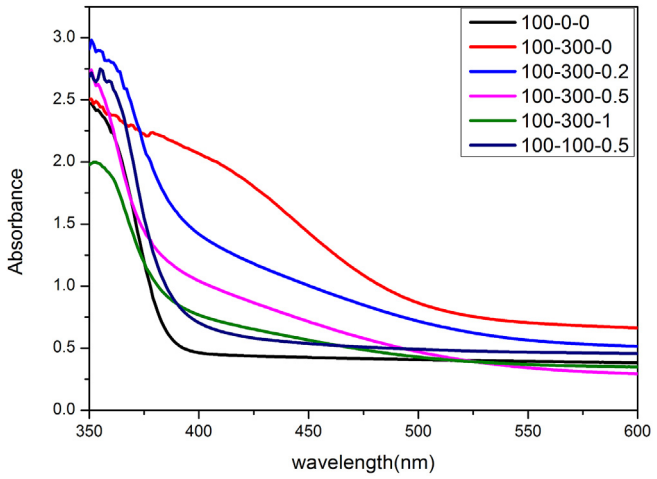

Fig. 4. UV–vis spectra of doped TiO_2 thin film.

3.2. Optical properties of the Y,N co-doped TiO_2 thin films

The TiO_2 powder turns into yellow after nitrogen doping, indicating that the optical properties of the samples have changed. As UV–vis spectrometry is often used to examine the optical structures and effects of dopants on metal oxide thin film, we scan the visible light absorption spectra herein to demonstrate the effects of incorporated dopants and the results are shown in Fig. 4. In Fig. 4, no absorption peak for pure TiO_2 is observed above 380 nm.

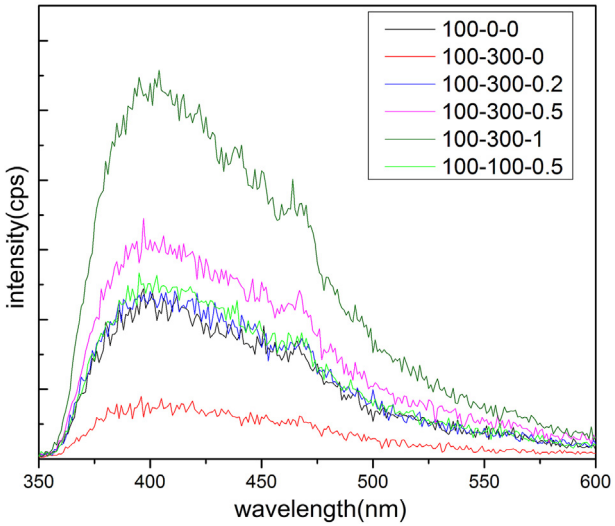

Fig. 5. PL intensities of TiO_2 nanoparticles at λ_{ex} = 325 nm.

However, doped samples all illustrate absorption redshift in the visible light region. For nitrogen doped only sample 100-300-0, we can find out the enhanced light absorption in the visible light area, which forms an obvious broadened peak stretched to 500 nm, featuring nitrogen doped TiO_2. This visible light activity is believed to be attributed to a new N 2p state close to the valance band maximum caused by nitrogen doping [39]. In the co-doped system, as the yttrium doping amount increases, the broadened peak of the nitrogen doped TiO_2 shrinks, i.e., the absorption edge of co-doped samples shows a small blue shift with the increased amount of Y^{3+}. For example, the absorbance of 100-300-0, 100-300-0.2, 100-300-0.5 and 100-300-1 at the same length of 400 nm is 2.07, 1.42, 1.04 and 0.77, respectively. As a result, powder with more yttrium doping reveals a paler yellow color.

To understand the efficiency of charge trapping and transfer in the semiconductor, we performed the photoluminescence (PL) measurements. The change of PL intensities can reveal the photo-generated charge-carrier recombination rate in semiconductors. In Fig. 5, the PL spectra of synthesized nanoparticles are recorded at $\lambda_{ex} = 325$ nm. As shown in Fig. 5, the PL spectra of TiO_2 possess two major peaks, which are around 410 nm and 465 nm, respectively. The broadened peak at 410 nm is attributed to the band gap recombination of TiO_2 and the peak at 465 nm is related with free-excition recombination emission [40,41]. As many previous researches [42,43] illustrate, the PL intensity of 100-300-0 with the nitrogen doped only sample decreases, which means the charge recombination is suppressed by incorporated nitrogen. On the other hand, the PL intensities of codoped samples increase when more yttrium is doped. This indicates that more defect sites, namely oxygen vacancies are introduced by yttrium doping, which serve as recombination centers [44]. Further analyses are discussed in the following XPS measurements.

3.3. Electronic structures of Y, N co-doped TiO_2 thin films

To probe the electronic structure and chemical environment of Y,N co-doped TiO_2, XPS surveys are investigated. For sample 100-100-0.5, the concentration of doped Y and N are confirmed to be 0.30% and 0.48% by XPS survey scan (see Fig. S3), respectively. All four elemental regions given by detail scan, the Ti 2p region around 460 eV (Fig. 6a and c), O1s region around 532 eV (Fig. 6b and d), Y 3d region around 160 eV (Fig. 6e) and N 1s region around 400 eV (Fig. 6f), are shown in Fig. 6, respectively.

In particular, the XPS detail scans are fitted with nonlinear Gaussian–Lorentzian peak shapes. In Fig. 6e, the two peaks at 158.1 eV and 160.2 eV are assigned to $3d_{5/2}$ and $3d_{3/2}$ states of Y^{3+}, which indicates the yttrium doping into the TiO_2 lattice. The XPS pattern of N 1s state shown in Fig. 6f indicates two peaks at about

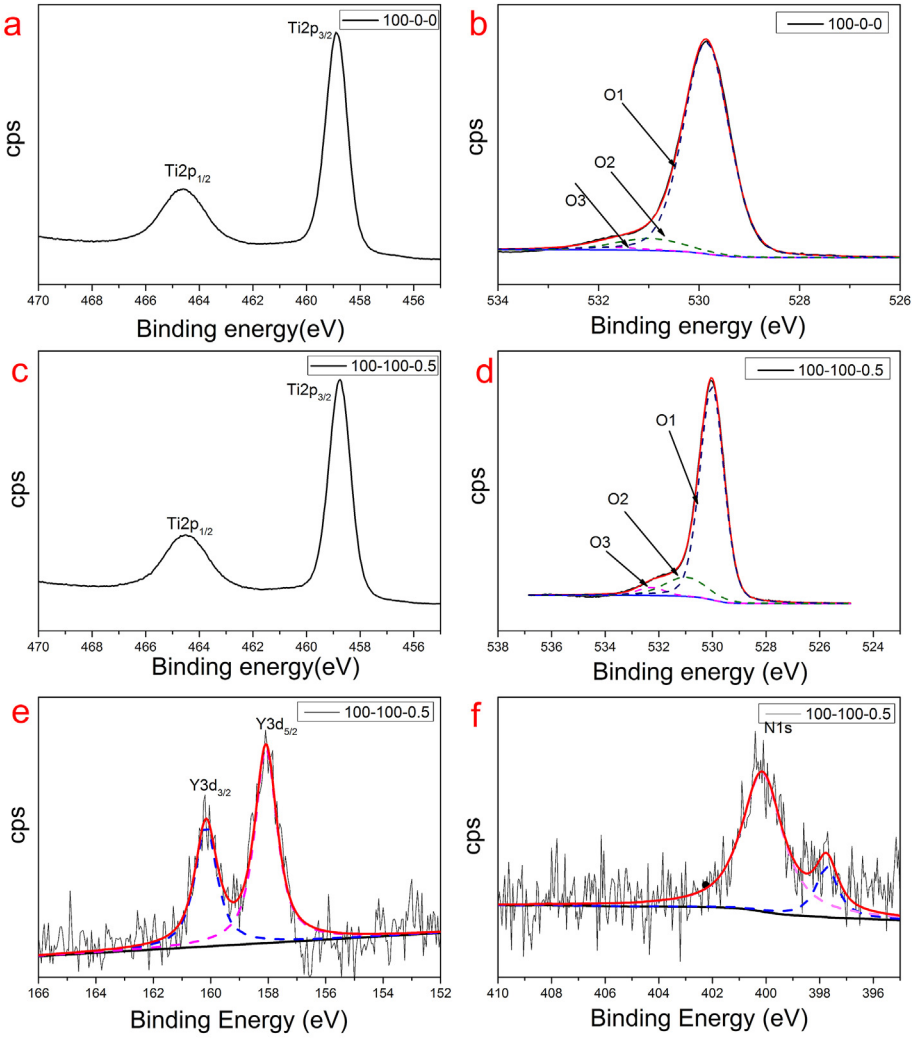

Fig. 6. XPS detailed scan of (a) Ti2p and (b) O1s of 100-0-0; (c) Ti2p, (d) O1s, (e) Y3d and (f) N1s of 100-100-0.5, respectively.

397.9 and 400.4 eV, which lie in the range of 396–404 eV observed by other authors [45,46]. According to previous researches, the peak at around 400 eV refers to chemically absorbed γ-N_2 [33]. But other peaks are considered to be related to the preparation method and chemical environment surrounded. For example, Burda et al. [47] indicated that, when nitrogen substitutes for the oxygen in the initial O–Ti–O structure, the electron density around N is reduced, and the N 1s binding energy in an O–Ti–N is higher than that in a N–Ti–N environment. Di Valentin et al. [48] used DFT calculation to clarify the binding energy of substitutional and interstitial N atom in TiO_2 matrix. In this case, the samples are synthesized via a sol–gel route, we regard the peak at 397.9 eV as an O–Ti–N structure. As the result of incorporated yttrium and nitrogen, the Ti 2p spectrum of co-doped sample differs from the pure one. In Fig. 6c, the peak of Ti $2p_{3/2}$ state in 100-100-0.5 slightly decreases for 0.13 eV after doping. Such decrease in Ti 2p binding energy can be due to the incorporated N. With the formation of O–Ti–N bond, the oxygen in TiO_2 is substituted by excess nitrogen. Therefore, the electron density around Ti atom increases, because the electronegativity of nitrogen is lower than oxygen [49]. Consequently, the binding energy of Ti decreases.

As shown in Fig 5. (b) and (d), the O1s core peak position shifts from 529.8 eV of 100-0-0 to 530.0 eV of 100-100-0.5, indicating that the chemical environment of this element has been changed [50]. Furthermore, oxygen 1s peaks can be de-convoluted into three peaks, namely O1, O2 and O3 [51,52]. The O1 peak at 530 eV refers to the oxygen bounded to Ti. The O2 peak at 531 eV refers to the oxygen deficient regions within the matrix of TiO_2. And the O3 peak is usually attributed to the chemisorbed species on the TiO_2 surface. As the peak data listed in Table 1 show, the O2 peak area, i.e. the defect level peak of oxygen, increased from 9.9% to 15.8% in the doped sample. Since the substitutional doping of yttrium into the TiO_2 lattice is a p-type doping, the increment of oxygen vacancies are supposed to keep the charge balance in the sample. The O1s scan of co-doped TiO_2 confirms our PL measurements that more oxygen vacancies are generated after doping.

3.4. Photovoltaic performances of DSSCs

The photovoltaic performances based on Y, N co-doped TiO_2 and pure TiO_2 are shown in Fig. 7 and Table 2. The co-doped DSSCs achieve improvements in light-to-electricity conversion efficiencies compared with traditional DSSCs fabricated by un-doped TiO_2 nanoparticles. In short, the sample 100-300-0.5 obtains 5.41% efficiency without any other post-treatment like dipping in the $TiCl_4$ solution, 18% higher than the pure TiO_2 electrodes. Compared to the 100-0-0 cell, although we observe that the doped ones have a smaller fill factor (FF), the enhancement of open circuit voltage (V_{oc}) and short circuit current density (J_{sc}) enables the doped cells reaching a better cell performance.

The increment of dye adsorption amount of the doped TiO_2 should be mainly responsible for enhancement of J_{sc}. To determine the dye adsorption amount, the NaOH-ethanol solution was used to desorb the dye loaded on the photoanodes and the absorbance of the N719 desorption solution at 520 nm were used to determine the

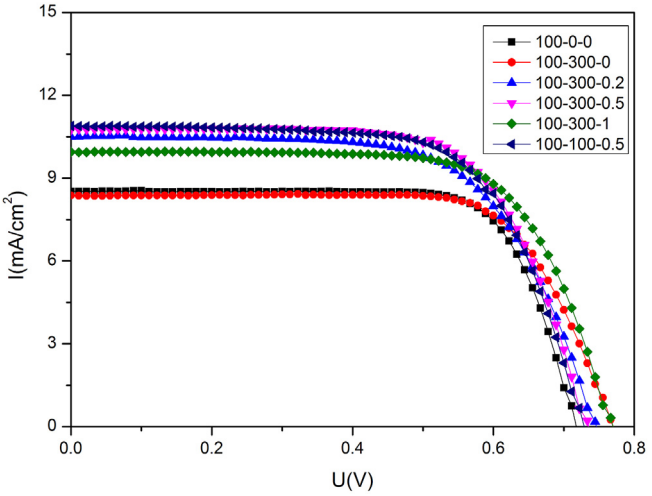

Fig. 7. Photocurrent-voltage characteristics of DSSCs assembled by doped TiO_2 electrodes.

adsorption amount. As Table 2 summarizes, the dye adsorption amount increases in the nitrogen doped sample 100-300-0, which is 1.32×10^{-7} mol/cm^2, 15.7% enhancement than the un-doped electrode; Furthermore, when yttrium doping concentration increases in the co-doped samples, the adsorption amount further increases. It increased to 2.19×10^{-7} mol/cm^2 in the co-doped 100-300-1 sample, which almost doubled after doping. According to BET measurements results, the BET surface area suggested that the co-doped nanoparticles own larger surface areas, which contribute to the enhanced dye adsorption amount. Additionally, Zeta potentials of the nanoparticles were also measured and listed in Table S1. The results show that the nanoparticles are negatively charged at pH 7, and zeta potential of the nitrogen doped sample is 2 mV higher than the un-doped one, which show same trends with previous research [53]. Furthermore, the charge of Y, N co-doped samples are about 3–8 mV smaller than nitrogen doped sample. It is known that TiO_2 exhibits amphoteric properties, because the surface Ti–OH structure can act as both basic and acid sites. When yttrium is also doped in the lattice, as the electronegativity of yttrium (1.22) is smaller than titanium (1.54), the Y–OH bond should act as a more basic site than Ti–OH, which also contributes to the increment of zeta potential [54]. As N719 dye is negatively charged as well with acidic carboxyl groups, the doped samples with fewer negative charges are believed to repel N719 to a smaller extent, thus facilitating higher dye loading ability. As a result, the highest J_{sc} occurred in 100-300-0.5, which reached 10.76 mA/cm^2.

In addition, although some former research papers indicated that nitrogen doping could generate sub-band near valence band maximum, other than changing the conduction band minimum [55] (approximately the quasi-Fermi level) of TiO_2 and influencing the V_{oc}, other perspectives, like Dai et al.'s [56] point out that, the flat band potential of their nitrogen doped TiO_2 electrode negatively shifted by 60–100 mV, which caused V_{oc} increment in the

Table 1
Summary of peak positions and areas of O1s detailed scan of 100-0-0 and 100-100-0.5

Peak name	100-0-0		100-100-0.5	
	Peak position (eV)	Peak area (%)	Peak position (eV)	Peak area (%)
O1	529.8	89.9	530.0	79.7
O2	531.0	9.9	530.8	15.8
O3	531.9	0.2	532.2	4.5

Table 2
Summary of detailed parameters of doped DSSCs.

Samples	V_{oc} (V)	J_{sc} (mA/cm^2)	FF (%)	EFF (%)	Dye adsorption amount ($\times 10^{-7}$ mol/cm^2)
100-0-0	0.718	8.52	74.6	4.58	1.14
100-300-0	0.769	8.37	71.6	4.61	1.32
100-300-0.2	0.745	10.50	64.5	5.05	1.69
100-300-0.5	0.735	10.76	68.4	5.41	1.69
100-300-1	0.769	10.05	69.4	5.36	2.19
100-100-0.5	0.729	10.88	66.8	5.30	1.70

cells. In this experiment, we find out that with nitrogen doping, the V_{oc} of DSSCs has increased about 20–40 mV, and the V_{oc} is higher in the samples with more nitrogen doped (0.735 V for 100-300-0.5 and 0.729 V for 100-100-0.5). Due to the complexity nature of nitrogen doping discussed above in section 3.3, we suggest that the differences may come from the different synthesis route, as the nitrogen binding energies and chemical states in TiO_2 varies from the preparation methods.

In the Y, N co-doped system, although we saw a slightly decrease of V_{oc} compared with N single doped, the J_{sc} increased for more than 20% compared with the single doped one, which could compensate for the decline of V_{oc}. The performances of DSSCs correspond well with PL measurements results that the nitrogen doped only TiO_2 have lower charge recombination than the co-doped samples. Although more severe recombination happens in the co-doped electrodes, the better dye adsorption ability of co-doped electrodes could transfer much more photo-generated electrons, thus the loss of V_{oc} is compensated by higher J_{sc}. As optimizing the co-doping level of nitrogen and yttrium, the cell reaches 5.41% of 100-300-0.5, about 18% higher than the pure 100-0-0 without any further post-treatment.

3.5. Electrochemical analysis of DSSCs

To further understand the effects of dopants on the TiO_2 electrodes and recombination in the cells, the EIS spectra of DSSCs fabricated by pure and doped TiO_2 based cell were measured in the condition of dark, open-circuit bias. And the Nyquist and Bode plots, the fitted parameters are shown in Fig. 8 and Table 3, respectively.

Typically, in the frequency range of this experiment (0.1–10 kHz), there are two semicircles in the Nyquist plots. The semicircle in the higher frequency zone refers to the charge transfer resistance at counter electrode, whereas another semicircle in the intermediate frequency zone refers to the charge transport resistance at the TiO_2/electrolyte interface (R_t). The decreased charge transport resistance meant restrained recombination in the cell. As R_t in Table 3 and semicircles in the Fig. 8a depicted, the doped samples all possessed *ca.* 40Ω charge transport resistance, which was much smaller than the pure sample (74.2Ω). The suppressed R_t is mainly due to the enhanced dye loading amount in the doped samples. Besides, the intersection of curve with Z′-axis is the cell's series resistance (R_s), which consists of sheet resistance of the FTO glass and contact resistance [57]. However, we saw a higher series resistance on the nitrogen doped sample 100-300-0, which should contribute to the nitrogen introduced into TiO_2 that increase the powder resistance [26].

Table 3
Summary of fitted EIS results of doped DSSCs.

Samples	R_s (Ω)	R_t (Ω)	τ_n (ms)
100-0-0	24.6	74.2	50.3
100-100-0.5	26.1	43.5	73.9
100-300-0	34.7	43.8	61.0
100-300-0.5	26.3	39.3	73.9

Moreover, from the Bode plots in Fig. 8b, two time constants are shown, and electron life time τ_n can be calculated by position of the low frequency peak through equation (1) [58]:

$$\tau_n = 1/2\pi f \quad (1)$$

where f means the frequency of superimposed ac voltage. The τ_n in co-doped sample 100-300-0.5 was 73.9 ms, much longer than that in the un-doped one of 50.3 ms.

Both the lower charge transfer resistance and longer electron life time illustrates the suppressed charge recombination. In this experiment, as the excess elements are slightly doped into the TiO_2 nanoparticles, the charge distribution in the particle is less than a few meV [59] and electron transport is dominated by diffusion in

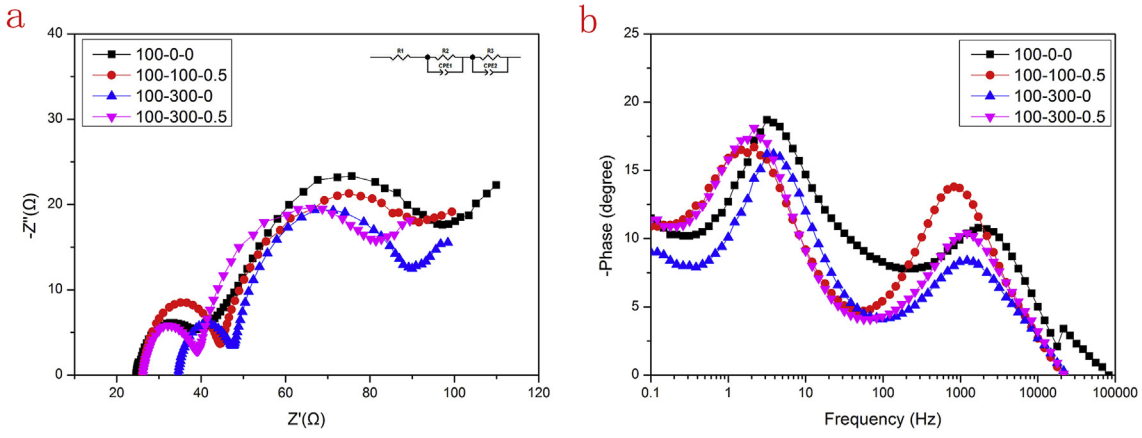

Fig. 8. EIS curves of DSSCs based on doped TiO_2 electrodes: (a) is the Nyquist plot with the inset of equivalent circuit and (b) is the Bode plot.

the mesoporous thin film. In other words, as Gregg et al. [60] pointed out previously, in the mesoporous TiO_2 thin film system, the surface charge recombination behavior strongly related to the Helmholtz layer capacitance of the porous thin film and electrolyte interface, which is linearly dependent on the effective surface area of the TiO_2 film. As the doped nitrogen and yttrium increased the surface area of the nanoparticles, the enhanced charge transfer behavior is expected in the co-doped TiO_2 mesoporous electrode. Hence, the EIS results mentioned above confirm the better performance of Y, N co-doped electrodes.

4. Conclusions

In summary, we used a facile sol–gel process to synthesize yttrium and nitrogen co-doped TiO_2 nanoparticles. Compared with pure TiO_2, doping causes E_g Raman vibration mode redshifted for ca. 2–4 cm^{-1} and broadening the light absorbance into visible light area. As incorporating yttrium with nitrogen, the BET surface area was further increased, which enhanced the dye uptake of the electrode and increased the J_{sc}. By tuning an optimized amount of doping concentration, a best light-to-electricity conversion efficiency of 5.41% was obtained in sample 100-300-0.5 without post-treatment on photoanode, which was 18% higher compared with pure TiO_2 electrode. As the EIS measurements indicated, the synergistic effect of yttrium and nitrogen co-doping TiO_2 suppressed the charge recombination in the cell. Therefore, the synthesized co-doped TiO_2 via a simple sol–gel method could be used as high performance photoanode for DSSC, which provides an example for potential use of other cation and anion co-doped TiO_2 in DSSCs.

Acknowledgments

This work was supported by the National Basic Research Program of China (2012CB932303) and the National Natural Science Foundation of China (Grant No. 51272265, 61574148).

Appendix A. Supplementary data

Supplementary data related to this article can be found at http://dx.doi.org/10.1016/j.jallcom.2015.10.254.

References

[1] B. Oregan, M. Gratzel, A Low-cost, high-efficiency solar-cell based on dye-sensitized colloidal TiO_2 films, Nature 353 (1991) 737–740.
[2] U. Bach, D. Lupo, P. Comte, J.E. Moser, F. Weissortel, J. Salbeck, H. Spreitzer, M. Gratzel, Solid-state dye-sensitized mesoporous TiO_2 solar cells with high photon-to-electron conversion efficiencies, Nature 395 (1998) 583–585.
[3] M. Gratzel, Photoelectrochemical cells, Nature 414 (2001) 338–344.
[4] M. Gratzel, Dye-sensitized solar cells, J. Photochem. Photobiol. C-Photochem. Rev. 4 (2003) 145–153.
[5] S.H. Hwang, J. Yun, J. Jang, Multi-shell porous TiO_2 hollow nanoparticles for enhanced light harvesting in dye-sensitized solar cells, Adv. Funct. Mater. 24 (2014) 7619–7626.
[6] S. Yang, Y.C. Zheng, Y. Hou, X.H. Yang, H.G. Yang, Anatase TiO_2 with nanopores for dye-sensitized solar cells, Phys. Chem. Chem. Phys. 16 (2014) 23038–23043.
[7] S.S. Mali, H.J. Kim, C.S. Shim, W.R. Bae, N.L. Tarwal, S.B. Sadale, P.S. Patil, J.H. Kim, C.K. Hong, Single-step synthesis of 3D nanostructured TiO_2 as a scattering layer for vertically aligned 1D nanorod photoanodes and their dye-sensitized solar cell properties, CrystEngComm 15 (2013) 5660–5667.
[8] B. Liu, E.S. Aydil, Growth of oriented single-crystalline rutile TiO_2 nanorods on transparent conducting substrates for dye-sensitized solar cells, J. Am. Chem. Soc. 131 (2009) 3985–3990.
[9] F. Shao, J. Sun, L. Gao, S.W. Yang, J.Q. Luo, Forest-like TiO_2 hierarchical structures for efficient dye-sensitized solar cells, J. Mater. Chem. 22 (2012) 6824–6830.
[10] V.M. Guérin, J. Rathousky, T. Pauporté, Electrochemical design of ZnO hierarchical structures for dye-sensitized solar cells, Sol. Energy Mater. Sol. Cells 102 (2012) 8–14.
[11] V. Kumar, N. Singh, V. Kumar, L.P. Purohit, A. Kapoor, O.M. Ntwaeaborwa, H.C. Swart, Doped zinc oxide window layers for dye sensitized solar cells, J. Appl. Phys. 114 (2013) 134506.
[12] J. Wang, Z.Q. Lin, Dye-sensitized TiO_2 nanotube solar cells with markedly enhanced performance via rational surface engineering, Chem. Mater. 22 (2010) 579–584.
[13] J. Bandara, U.W. Pradeep, Tuning of the flat-band potentials of nanocrystalline TiO_2 and SnO_2 particles with an outer-shell mgo layer, Thin Solid Films 517 (2008) 952–956.
[14] A. Marchioro, A. Dualeh, A. Punzi, M. Grätzel, J.E. Moser, Effect of posttreatment of titania mesoscopic films by $TiCl_4$ in solid-state dye-sensitized solar cells: a time-resolved spectroscopy study, J. Phys. Chem. C 116 (2012) 26721–26727.
[15] M.J. Robles-Aguila, M.E. Mendoza, M.M. Davila-Jimenez, U. Bentrup, M.P. Elizalde-Gonzalez, Influence of Ni Doping on the structural, optical and textural properties of TiO_2 nanocrystals prepared via an ultrasound assisted sol-gel method, J. Sol-Gel Sci. Technol. 69 (2014) 571–579.
[16] X. Lü, X. Mou, J. Wu, D. Zhang, L. Zhang, F. Huang, F. Xu, S. Huang, Improved-performance dye-sensitized solar cells using Nb-doped TiO2 electrodes: efficient electron injection and transfer, Adv. Funct. Mater. 20 (2010) 509–515.
[17] W.X. Li, J.Y. Yang, J.Q. Zhang, S. Gao, Y.B. Luo, M. Liu, Improve photovoltaic performance of titanium dioxide nanorods based dye-sensitized solar cells by Ca-doping, Mater. Res. Bull. 57 (2014) 177–183.
[18] S. Sadhu, P. Poddar, Growth of oriented single crystalline La-doped TiO_2 nanorod arrays electrode and investigation of optoelectronic properties for enhanced photoelectrochemical activity, RSC Adv. 3 (2013) 10363–10369.
[19] R. Valaski, C. Arantes, C.A. Senna, V. Carôzo, C.A. Achete, M. Cremona, Enhancement of open-circuit voltage on organic photovoltaic devices by Al-doped TiO_2 modifying layer produced by sol–gel method, Thin Solid Films 572 (2014) 2–7.
[20] S. Sood, A. Umar, S.K. Mehta, S.K. Kansal, Highly effective Fe-doped TiO_2 nanoparticles photocatalysts for visible-light driven photocatalytic degradation of toxic organic compounds, J. Colloid And Interface Sci. 450 (2015) 213–223.
[21] E.M. Hopper, F. Sauvage, A.K. Chandiran, M. Graetzel, K.R. Poeppelmeier, T.O. Mason, Electrical properties of Nb-, Ga-, and Y-substituted nanocrystalline anatase TiO_2 prepared by hydrothermal synthesis, J. Am. Ceram. Soc. 95 (2012) 3192–3196.
[22] M.A. Baker, H. Fakhouri, R. Grilli, J. Pulpytel, W. Smith, F. Arefi-Khonsari, Effect of total gas pressure and O_2/N_2 flow rate on the nanostructure of N-doped TiO_2 thin films deposited by reactive sputtering, Thin Solid Films 552 (2014) 10–17.
[23] S. Sakthivel, H. Kisch, Daylight photocatalysis by carbon-modified titanium dioxide, Angew. Chem. Int. Ed. 42 (2003) 4908–4911.
[24] J.C. Yu, J.G. Yu, W.K. Ho, Z.T. Jiang, L.Z. Zhang, Effects of F- doping on the photocatalytic activity and microstructures of nanocrystalline TiO_2 powders, Chem. Mater. 14 (2002) 3808–3816.
[25] T. Ohno, M. Akiyoshi, T. Umebayashi, K. Asai, T. Mitsui, M. Matsumura, Preparation of S-doped TiO_2 photocatalysts and their photocatalytic activities under visible light, Appl. Catal. a-General 265 (2004) 115–121.
[26] W. Guo, Y. Shen, L. Wu, Y. Gao, T. Ma, Effect of N dopant amount on the performance of dye-sensitized solar cells based on N-doped TiO_2 electrodes, J. Phys. Chem. C 115 (2011) 21494–21499.
[27] T.L. Ma, M. Akiyama, E. Abe, I. Imai, High-efficiency dye-sensitized solar cell based on a nitrogen-doped nanostructured titania electrode, Nano Lett. 5 (2005) 2543–2547.
[28] W. Guo, Y. Shen, G. Boschloo, A. Hagfeldt, T. Ma, Influence of nitrogen dopants on N-doped TiO_2 electrodes and their applications in dye-sensitized solar cells, Electrochimica Acta 56 (2011) 4611–4617.
[29] J. Zhu, Z. Deng, F. Chen, J. Zhang, H. Chen, M. Anpo, J. Huang, L. Zhang, Hydrothermal Doping Method for Preparation of Cr3+-TiO2 Photocatalysts with Concentration Gradient Distribution of Cr^{3+}, Appl. Catal. B Environ. 62 (2006) 329–335.
[30] H. Irie, Y. Watanabe, K. Hashimoto, Nitrogen-concentration dependence on photocatalytic activity of TiO_2-xN_x powders, J. Phys. Chem. B 107 (2003) 5483–5486.
[31] Q. Meng, T. Wang, E. Liu, X. Ma, Q. Ge, J. Gong, Understanding electronic and optical properties of anatase TiO2 photocatalysts Co-doped with nitrogen and transition metals, Phys. Chem. Chem. Phys. 15 (2013) 9549–9561.
[32] W. Zhu, X. Qiu, V. Iancu, X.-Q. Chen, H. Pan, W. Wang, N.M. Dimitrijevic, T. Rajh, H.M. Meyer III, M.P. Paranthaman, G.M. Stocks, H.H. Weitering, B. Gu, G. Eres, Z. Zhang, Band gap narrowing of titanium oxide semiconductors by noncompensated anion-cation codoping for enhanced visible-light photoactivity, Phys. Rev. Lett. 103 (2009).
[33] Z. Bi, M.P. Paranthaman, B. Guo, R.R. Unocic, H.M.I. Meyer, C.A. Bridges, X. Sun, S. Dai, High performance Cr, N-codoped mesoporous TiO_2 microspheres for lithium-ion batteries, J. Mater. Chem. A 2 (2014) 1818–1824.
[34] P. Qin, A.L. Domanski, A.K. Chandiran, R. Berger, H. Butt, M.I. Dar, T. Moehl, N. Tetreault, P. Gao, S. Ahmad, M.K. Nazeeruddin, M. Graetzel, Yttrium-substituted Nanocrystalline TiO_2 photoanodes for Perovskite based heterojunction solar cells, Nanoscale 6 (2014) 1508–1514.
[35] A.K. Chandiran, F. Sauvage, L. Etgar, M. Graetzel, Ga^{3+} and Y^{3+} Cationic substitution in mesoporous TiO_2 photoanodes for photovoltaic applications, J. Phys. Chem. C 115 (2011) 9232–9240.
[36] S. Ito, T.N. Murakami, P. Comte, P. Liska, C. Graetzel, M.K. Nazeeruddin, M. Graetzel, Fabrication of thin film dye sensitized solar cells with solar to

electric power conversion efficiency over 10%, Thin Solid Films 516 (2008) 4613–4619.
[37] J. Zhang, M.J. Li, Z.C. Feng, J. Chen, C. Li, UV Raman spectroscopic study on TiO_2. I. Phase transformation at the surface and in the bulk, J. Phys. Chem. B 110 (2006) 927–935.
[38] H. Zhang, K. Tan, H. Zheng, Y. Gu, W.F. Zhang, Preparation, characterization and photocatalytic activity of TiO2 codoped with yttrium and nitrogen, Mater. Chem. Phys. 125 (2011) 156–160.
[39] N. Serpone, Is the band gap of pristine TiO_2 narrowed by anion- and cation-doping of titanium dioxide in second-generation photocatalysts? J. Phys. Chem. B 110 (2006) 24287–24293.
[40] Y. Wang, H. Yang, X. Xue, Synergistic antibacterial activity of TiO2 co-doped with zinc and yttrium, Vacuum 107 (2014) 28–32.
[41] J.C. Yu, Yu, Ho, Jiang, Zhang, Effects of F- Doping on the Photocatalytic Activity and Microstructures of Nanocrystalline TiO2 Powders, Chem. Mater. 14 (2002) 3808–3816.
[42] B. Liu, L. Wen, X. Zhao, The structure and photocatalytic studies of N-doped TiO2 films prepared by radio frequency reactive magnetron sputtering, Sol. Energy Mater. Sol. Cells 92 (2008) 1–10.
[43] X. Liu, Z. Liu, J. Zheng, X. Yan, D. Li, S. Chen, W. Chu, Characteristics of N-doped TiO2 nanotube arrays by N2-plasma for visible light-driven photocatalysis, J. Alloy. Compd. 509 (2011) 9970–9976.
[44] H. Zhang, G. Miao, X. Ma, B. Wang, H. Zheng, Enhancing the photocatalytic activity of nanocrystalline TiO2 by co-doping with fluorine and yttrium, Mater. Res. Bull. 55 (2014) 26–32.
[45] D.J.V. Pulsipher, I.T. Martin, E.R. Fisher, Controlled nitrogen doping and film colorimetrics in porous TiO2 materials using plasma processing, ACS Appl. Mater. Interfaces 2 (2010) 1743–1753.
[46] X. Wang, Y. Yang, Z. Jiang, R. Fan, Preparation of TiN_xO_{2-x} photoelectrodes with NH_3 under controllable middle pressures for dye-sensitized solar cells, Eu. J. Inorg. Chem. (2009) 3481–3487.
[47] C. Burda, Y. Lou, X. Chen, A.C.S. Samia, J. Stout, J.L. Gole, Enhanced nitrogen doping in TiO_2 nanoparticles, Nano Lett. 3 (2003) 1049–1051.
[48] C. Di Valentin, G. Pacchioni, A. Selloni, S. Livraghi, E. Giamello, Characterization of paramagnetic species in N-doped TiO_2 powders by EPR spectroscopy and DFT calculations, J. Phys. Chem. B 109 (2005) 11414–11419.
[49] J. Wang, W. Zhu, Y. Zhang, S. Liu, An efficient two-step technique for nitrogen-doped titanium dioxide synthesizing: visible-light-induced photodecomposition of methylene blue, J. Phys. Chem. C 111 (2007) 1010–1014.
[50] B. Zhao, J. Wang, H. Li, H. Wang, X. Jia, P. Su, The influence of yttrium dopant on the properties of anatase nanoparticles and the performance of dye-sensitized solar cells, Phys. Chem. Chem. Phys. 17 (2015) 14836–14842.
[51] V. Kumar, O.M. Ntwaeaborwa, J. Holsa, D.E. Motaung, H.C. Swart, The role of oxygen and titanium related defects on the emission of TiO2:Tb3+ nano-phosphor for blue lighting applications, Opt. Mater. 46 (2015) 510–516.
[52] K. Vinod, H.C. Swart, G. Mukut, C.B.B. Barend, A.J.V. Vuuren, M. Lee, O.M. Ntwaeaborwa, The role of neutral and ionized oxygen defects in the emission of tin oxide nanocrystals for near white light application, Nanotechnology 26 (2015) 295703.
[53] K. Bubacz, B. Tryba, A.W. Morawski, The Role of adsorption in decomposition of dyes on TiO_2 and N-modified TiO_2 photocatalysts under UV and visible light irradiations, Mater. Res. Bull. 47 (2012) 3697–3703.
[54] H.V. Fajardo, E. Longo, E.R. Leite, R. Libanori, L.F. Dias Probst, N.L. Villarreal Carreno, Synthesis, characterization and catalytic properties of nanocrystaline Y_2O_3-coated TiO_2 in the ethanol dehydration reaction, Mater. Research-Ibero-American J. Mater. 15 (2012) 285–290.
[55] T. Lindgren, J.M. Mwabora, E. Avendano, J. Jonsson, A. Hoel, C.G. Granqvist, S.E. Lindquist, Photoelectrochemical and optical properties of nitrogen doped titanium dioxide films prepared by reactive DC magnetron sputtering, J. Phys. Chem. B 107 (2003) 5709–5716.
[56] H.J. Tian, L.H. Hu, C.N. Zhang, W.Q. Liu, Y. Huang, L. Mo, L. Guo, J. Sheng, S.Y. Dai, Retarded charge recombination in dye-sensitized nitrogen-doped TiO_2 solar cells, J. Phys. Chem. C 114 (2010) 1627–1632.
[57] Q. Wang, J.E. Moser, M. Gratzel, Electrochemical impedance spectroscopic analysis of dye-sensitized solar cells, J. Phys. Chem. B 109 (2005) 14945–14953.
[58] R. Kern, R. Sastrawan, J. Ferber, R. Stangl, J. Luther, Modeling and interpretation of electrical impedance spectra of dye solar cells operated under open-circuit conditions, Electrochimica Acta 47 (2002) 4213–4225.
[59] L.M. Peter, Dye-sensitized nanocrystalline solar cells, Phys. Chem. Chem. Phys. 9 (2007) 2630–2642.
[60] A. Zaban, A. Meier, B.A. Gregg, Electric potential distribution and short-range screening in nanoporous TiO_2 electrodes, J. Phys. Chem. B 101 (1997) 7985–7990.